SPATIOTEMPORAL ANALYSIS OF PASSIVE MICROWAVE REMOTE SENSING DATA FOR RAPID DETECTION OF LARGE SCALE FLOOD MAPPING - A GEOSPATIAL APPROACH

Venkata Sai Krishna Vanama[1], Y. S. Rao[2]
[1] Centre for Urban Science and Engineering, Indian Institute of Technology Bombay, Mumbai 400076, India,
Email: vsaikrishna1990@gmail.com
[2] Centre of Studies in Resources Engineering, Indian Institute of Technology Bombay, Mumbai 400076, India,
Email: ysrao@iitb.ac.in

KEYWORDS: Land Surface Water Coverage, Spatial variability, AMSR-E, NDPI, Anomaly

ABSTRACT: Land Surface Water Coverage (LSWC) is one of the critical parameters in large-scale flood identification and agriculture monitoring. In this paper, a time series geospatial database of LSWC was created to analyse the large-scale flooding pattern. Normalized Difference polarization Index (NDPI) was computed from AMSR-E brightness temperature of vertical and horizontal polarizations at 36.5 GHz frequency. NDPI anomaly was created by using different methods such as anomalies based on a reference year and multi-annual average (absolute, relative and standardized). Also, an image similarity was calculated by using Bhattacharya distance to extract the hidden information and similarities in the temporal images. Based on the similarity values, all the images in the database were ranked for rapid flood information extraction. The data used in the research include freely available AMSR-2 (2012-present) Passive Microwave Remote Sensing (MRS) data. The study area of the research covers the entire Tamil Nadu state of India. As Tamil Nadu is a coastal area, a buffer region from the coastline was created to identify the spatial variability of LSWC. The results show that there is a significant spatial variability of LSWC and also able to identify the major flood events. Also, the anomalies were helped to identify the geographic locations of flood hotspots at specific times during the flood events. Various anomalies were helped to identify the trend and pattern of flooding throughout the study area.

1 INTRODUCTION

Flood disasters are increasing globally and resulted in numerous losses. Climate change and population growth are the major driving factors to this phenomenon. Geospatial flood maps are the major tools for the preparation of emergency disaster response plan. These maps provide the crucial flood information such as the spatial extent of a flood event, people/crops affected, depth of flood water, flood losses, etc. Passive Microwave Remote Sensing (MRS) plays a major role in collecting the data due to the penetration of microwave signal through the clouds. Passive MRS provides spatiotemporal images for monitoring and analyzing the large-scale flood events. The difference of Vertical (V) and Horizontal (H) polarizations at 37 GHz frequency was preferable (Choudhury & Tucker 1987) to identify the flooding effects occurred in the Amazon River. For several flood events of Amazon River and other floodplains of South American rivers, the differencing algorithm (Sippel et al. 1994) applied to V and H polarizations at 37 GHz frequency measured by SMMR, was used to find the spatial extent of the flood area. Some studies also mention that Polarization Difference (PD = T_{bv} - T_{bh}) (Choudhury 1991) is largely influenced by vegetation cover and atmospheric conditions. Indices such as Polarization Ratio (PR = (T_{bv} - T_{bh})/(T_{bv} + T_{bh})) (Kerr & Njoku 1993) (Paloscia et al. 2001), Water Surface Fraction (*WSF*) (Zheng et al. 2008), Normalized Difference Frequency Index (NDFI) (Takeuchi & Gonzalez 2009), Wetness Index (WI) (Temimi et al. 2007), Water Surface Ratio (WSR) (Tanaka et al. 2003), Polarization Index (PI = (T_{bv} − T_{bh})/[0.5(T_{bv} + T_{bh})]) (Singh et al. 2013), Normalized Difference Polarization Index (NDPI) (Li & Takeuchi 2016) (Xi & Takeuchi 2015), land surface fractional open water (f_w) (Du et al. 2016), Polarization Ratio Variation Index (PRVI) (Lacava et al. 2015) were used by the researchers for flood mapping and soil moisture estimation. The PR is less affected by atmospheric conditions, and also it is independent of effective soil temperature. NDFI is also a good indicator of water coverage on the land surface, and this index can distinguish both land and water surfaces. A study conducted by (Watts et al. 2012) on AMSR-E f_w within the Arctic-Boreal Region is in strong agreement with regional monsoon cycles observed by basin discharge stations. Land Surface Water Coverage (LSWC) developed by (LI Xi & Wataru TAKEUCHI 2014) combining both AMSR-E and MODIS (Moderate Resolution Imaging Spectroradiometer) was useful for predicting the flood events. It is also identified that MODIS cannot detect the large scale flooding due to attenuation by the atmospheric window. The image similarity calculated by Bhattacharya distance (LI Xi & Wataru Takeuchi) was very useful in rapid extraction of flood information.

Advanced Microwave Scanning Radiometer 2 (AMSR-2), a passive MRS sensor onboard GCOM-W satellite launched by Japan is acquiring the data globally from July 02, 2012. Before this Advanced Microwave Scanning Radiometer-Earth Observing System (AMSR-E), onboard AQUA satellite had acquired the data globally form June 06, 2002 to Oct 04, 2011. This data can be freely obtained from JAXA website. With the launch of AMSR-2 which acquires the data at various frequencies and polarizations, there is a huge scope of rapid mapping of large-scale flood

events. The main objective of the research is to identify the potential of AMSR-2 in large-scale flood identification and to create the flood anomalies to identify the flood hotspots.

2 STUDY AREA AND DATASETS USED

The study area of the research shown in Figure 1 includes entire Tamil Nadu state of India which extended from 76.23ºE to 80.35ºE longitudes and 8.08ºN to 13.56ºN latitudes. Tamil Nadu state has 32 districts as per the 2011 census with a total area of about 130,058 km^2. The major rivers flow through the state includes Palar, Cauvery, Vaigai, Ponnaiyar, and Varattar. Also, Tamil Nadu has the second largest coastline of about 1,076 km in the country.

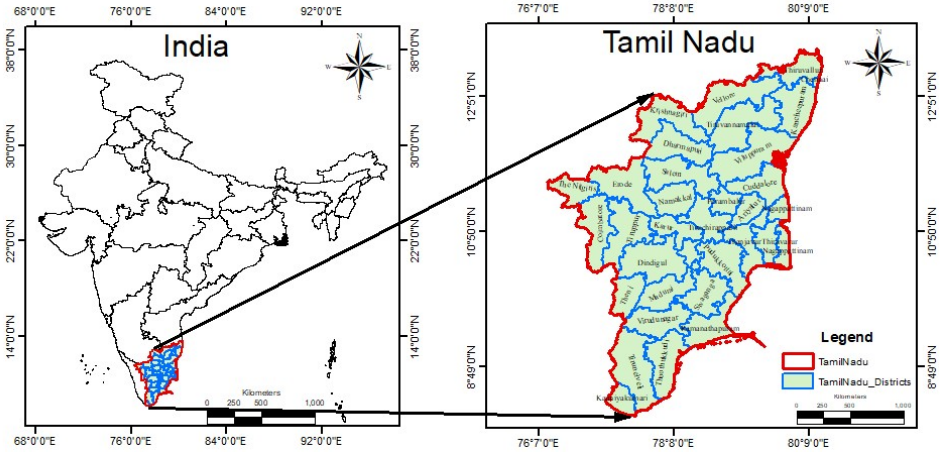

Figure 1: Study area showing India map and southern state Tamil Nadu.

List of flood events occurred in the state were collected from various secondary sources and found that the state has experienced two major flood events from Jan 2012 to Aug 2017. One of which happened on 01/11/2012 as shown in Figure 2a. The southern parts of the state were mainly affected by this flood and incurred huge losses. Another major flood event took place during 30th Nov-1st Dec 2015 in and around Chennai city as shown in Figure 2b. Chennai flood resulted in the heavy destruction of lifeline networks of the city. The cyan colour in Figure 2 shows the flood-affected areas.

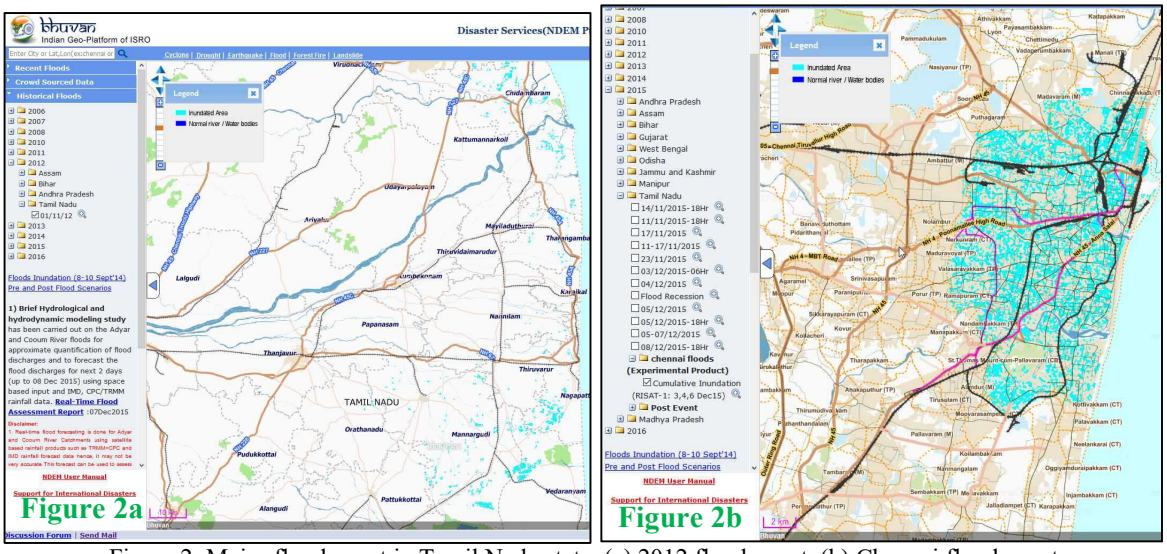

Figure 2: Major flood event in Tamil Nadu state. (a) 2012 flood event, (b) Chennai flood event

Spatio-temporal datasets of Level-3 AMSR-2 Brightness Temperature (T_b) acquired with horizontal (H) and vertical (V) polarization at 36.5 GHz frequencies from 2012 to 2017 were used for regional level flood event detection, i.e. at a state level. Level-3 AMSR-2 T_b is available at a spatial resolution of 10x10 km^2 and a 0.5-day temporal resolution. Globally every day the sensor acquires through one ascending and descending passes. For bulk acquisitions of temporal AMSR-2 images, subsetting of the data is not available on JAXA website. So, the entire world images were obtained from JAXA and these images were clipped to the study area extent. In the clipping operation, the parameters such as cell size, processing extent, no data values and image file formats are kept same to maintain the consistency of the database. Apart from the satellite datasets, the Tamil Nadu state and district boundary shapefiles were obtained from Data Meet warehouse which was created under GNU license.

3 METHODOLOGY AND ANALYSIS

The methodology is divided into two parts, the first part deals with pre-processing and analysis of spatiotemporal AMSR-2 images, whereas second part deals with flood hotspot detection using flood anomalies.

3.1 Spatio-temporal analysis of AMSR-2 data

All the temporal images of level-3 AMSR-2 were calibrated to calculate the T_b. The calibration factor 0.01 given in the AMSR-2 user manual was multiplied with the data values to get the correct temperature in Kelvin. The ascending and descending pass images are averaged to get the daily AMSR-2 images for each polarization respectively. All the computation on the images is performed by pixel-to-pixel basis. In the process of generating the daily images and further analysis, the No-data values are not considered. The daily AMSR-2 images were used to generate the Normalized Difference Polarization Index (NDPI) by using the formula $NDPI = (T_{b36.5V} - T_{b36.5H}) / (T_{b36.5V} + T_{b36.5H})$ where V, H refers to vertical and horizontal polarizations and 36.5 GHz refers to the frequency of the emitted microwave signal to capture the flood. This index is not affected by atmospheric conditions and sensitive to the water coverage. So, the index can distinguish the land and water surfaces for effective identification. The index values are ranging from -1 to +1. For better interpretation of the information, a minimum-maximum normalization technique was applied to the index to create LSWC database from 2012 to 2017 of the study area. LSWC represents the fraction of water coverage on the land surface with the values ranging from 0-100. Any land use category with higher LSWC values can be inferred as flood-affected regions and vice versa. The high moisture content on the ground surface results in low BT values (Choudhury & Pampaloni 1995) in horizontal polarization than the vertical recorded by the emitted microwave signal. In addition to the flood mapping applications, LSWC also plays a major role in soil moisture mapping, crop growth monitoring and drought area identification. Time series plots of AMSR-2 images with daily, monthly and yearly frequencies are created.

4 RESULTS AND DISCUSSIONS

4.1 Flood detection from AMSR-2 images

To understand the effect of trend and seasonality on the large-scale flood detection, time series AMSR-2 plots with varying frequencies of time are created. The spatial variation of daily LSWC average for the years 2012-2017 is shown in Figure 3. The red and green colour vowels in the figure represent the 2012 and Chennai flood events.

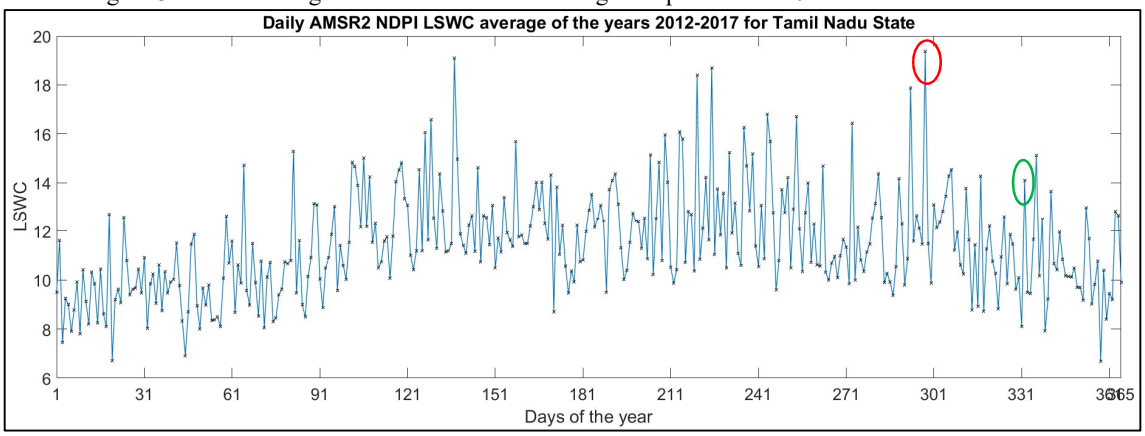

Figure 3: Averaged daily spatial variation of LSWC for the years 2012-2017.

The spatial variation of daily LSWC average is created by pixel-by-pixel averaging of same day images for all the years. The daily spatiotemporal distribution of LSWC throughout the study area shows an increase in the monsoon season. From the Figure 3, it is also observed that there is a fluctuation in the LSWC in the monsoon season. The high peaks in the monsoon may be the result of high rainfall or the presence of big water bodies. Also, there is a sudden a peak in the May month which needs a special investigation to find whether it is a noise data or may be the result of extreme events. The 2012 flood is easily detectable from the daily plot, whereas the Chennai flood is not highlighted. To analyze the Chennai flood further, geospatial analysis with data mining algorithms are required.

The second level of aggregation, i.e. the monthly analysis is carried out to explore the seasonal level similarities in the LSWC database. The spatial variation of monthly LSWC average is created by pixel-by-pixel averaging of same month images for all the years. The scatter plot shown in the Figure 4a of year by year monthly LSWC average for the years 2012-2017. For the year 2012, the data is available from July month, and for the year 2017, the data is considered up to August. So, the first and last year in the database is not considered for the seasonality trend identification. From the figure, it is observed that the LSWC values of 2013 and 2014, 2015 and 2016 are following

a similar trend and also 2013-2014 LSWC values are higher than the 2015-2016. For the further understanding of monthly LSWC variation, the monthly LSWC average for the years 2012-2017 is plotted in the Figure 4b. It is identified that the monsoon season has the high LSWC values as shown in a green colour vowel.

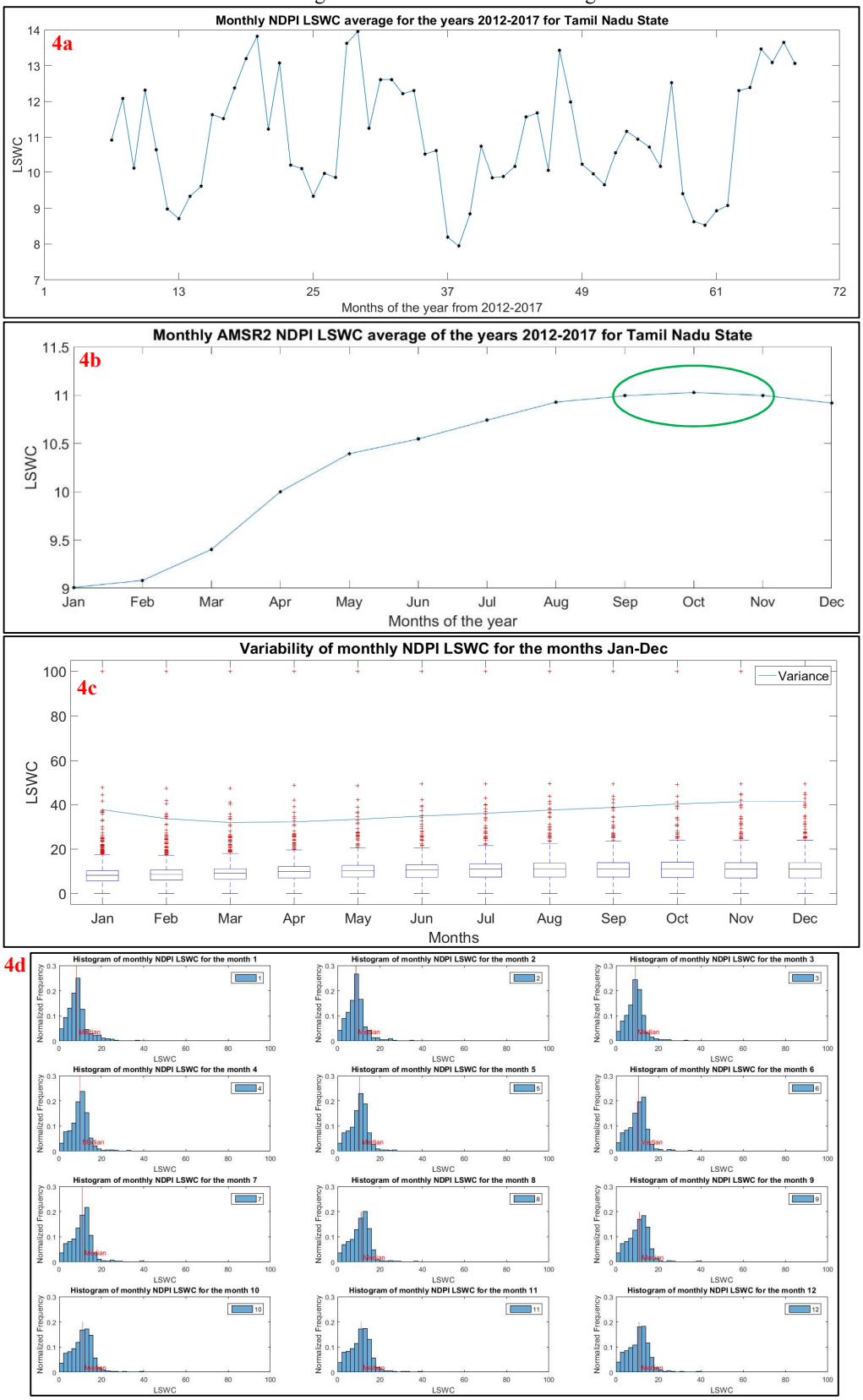

Figure 4: Average monthly spatial variation of LSWC for the years 2012-2017.

To understand the variability in the monthly LSWC data, the box plot and the histogram with normalized frequency are created as shown in Figure 4c and Figure 4d. From these figures, it is identified that the overall variability in the monthly LSWC is less. Also, the monsoon season images have the higher values than the other months. The spatial variation of monthly LSWC average is shown in Figure 5.

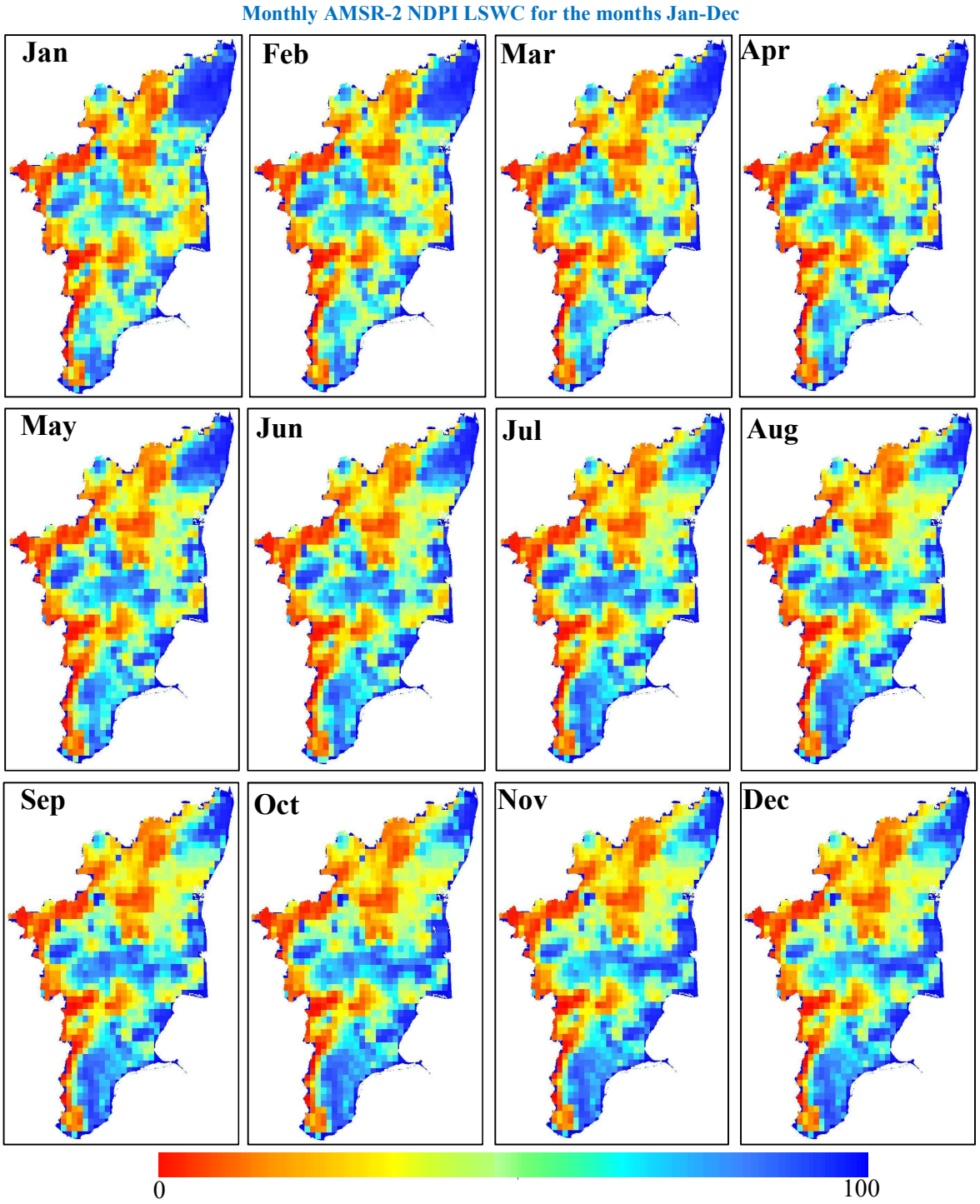

Figure 5: Spatial variation of monthly LSWC for the years 2012-2017.

The red and blue colour represents the zero and 100% LSWC respectively. For most of the months in a year, the coastal area of the state has higher LSWC values due to low elevation and water discharge through the area into the sea. It is also identified that there is low spatial variation which might be due to coarse resolution of AMSR-2 images. Therefore, the two flood events are difficult to identify from the spatial variation of monthly plots.

The third level of aggregation, i.e. the yearly analysis is carried out to study the yearly variation of LSWC values. The spatial variation of yearly LSWC average is created by pixel-by-pixel averaging of same year images for all the years. Figure 6a and 6b show the yearly variation and spatial distribution of LSWC for the years 2012-2017.

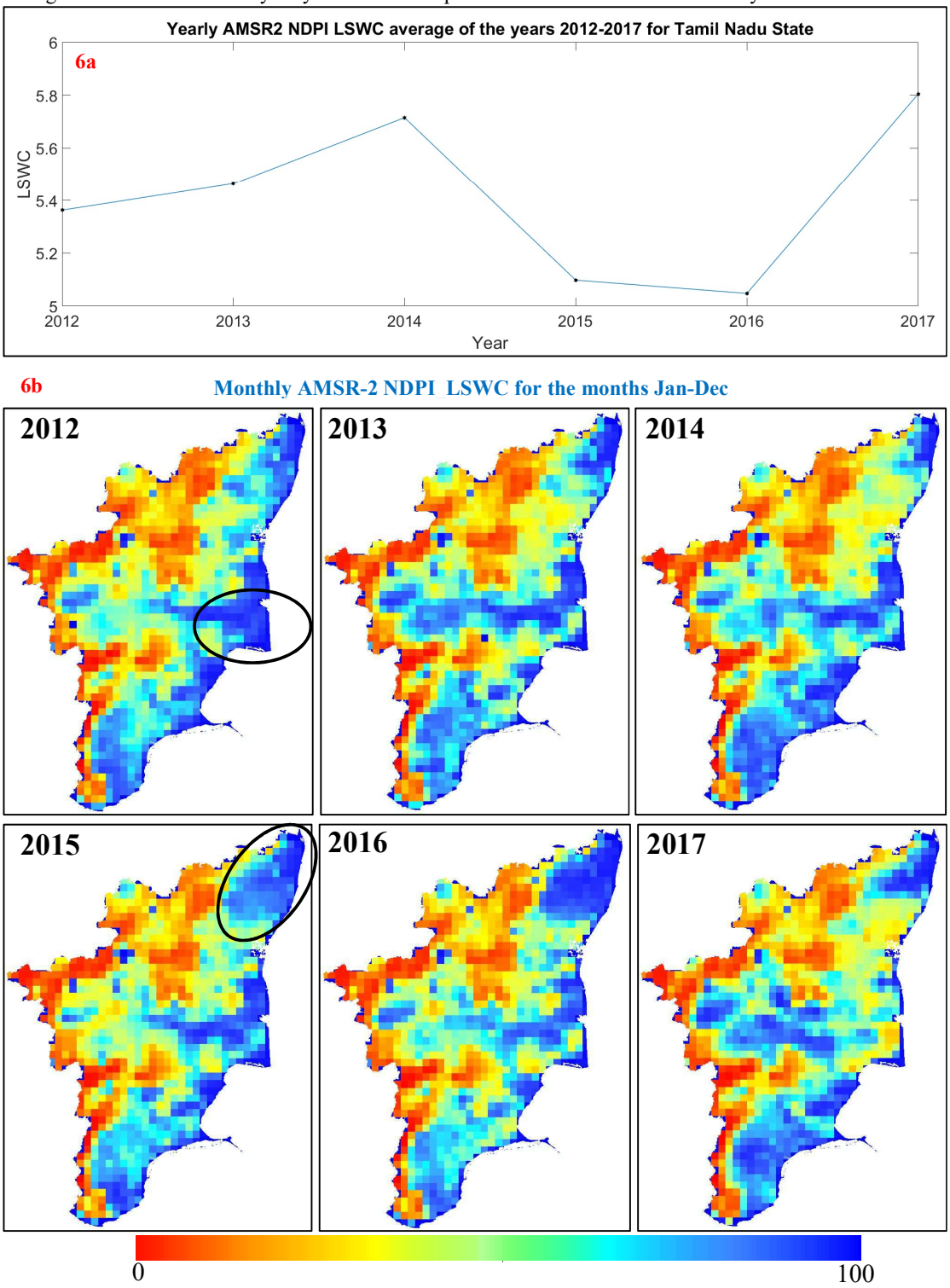

Figure 6: Spatial variation of yearly LSWC for the years 2012-2017.

The 2012 and Chennai flood events are identified in the yearly analysis which is highlighted in a black vowel. From all the time series plots, it is observed that third level of spatial aggregation of data is sensitive to large-scale flood events. The low values of 2015 LSWC shown in Figure 6a are attributed to spatial averaging and less variability of the data. In all the time series plotting, missing data is omitted.

4.2 Image similarity calculation

Image similarity plays a crucial role in rapid flood information retrieval. To identify the hidden similarities in the LSWC geodatabase, the highest LSWC value image is chosen as a master image. All the images in the database are compared with the master image with the help of Bhattacharya distance to calculate the Image similarity. The similarity values are assigned to images based on the distance, the lesser the distance, the better match with the master image. The images are ranked based on the similarity values. From the results, it is found that high similarity values are assigned to monsoon images. The Chennai flood image of 3rd Dec 2015 has got the similarity value with 0.7269 and ranked as the 12th image in the entire database.

4.3 LSWC anomaly

To find the flood hotspots, LSWC anomalies are created with based on a reference year, multi-annual average (absolute, relative and standardized). All the anomalies are created for yearly averaged data because it is identified as sensitive to large-scale flood mapping. In the reference year method, a reference year (2014) was selected based on the high variance in the data, and simple differencing approach is used. For the multi-annual average method, a four-year average is subtracted from every year. From the results of LSWC anomalies, the coastal areas are identified as the most vulnerable of the state.

5 CONCLUSIONS

In this paper, LSWC has derived from passive coarse resolution AMSR-2 T_b. The daily LSWC geodatabase for the years 2012-2017 has been created. It is proved that LSWC geodatabase has a great synergy for identification of the spatial and temporal components of various flood events at the regional level. Third level spatiotemporal aggregation is suitable for large-scale flood event detection. Also, Image similarity helps in raking the images for rapid flood information extraction. The results of coarse resolution AMSR-2 LSWC images appear to a slight underestimation of Chennai flood. The floods in an urban area are slightly under by the passive AMSR-2 images.

Acknowledgements

The first author is thankful to the Ministry of Human Resource Development, GoI for providing necessary computational facilities through the project 14MHRD005 funding. Authors are thankful to JAXA for providing the AMSR-2 data. We thank Head C-USE, IIT Bombay for his support throughout the research.

6 REFERENCES

Choudhury BJ. 1991. Passive microwave remote sensing contribution to hydrological variables. Surv Geophys. 12:63–84.

Choudhury BJ, Pampaloni P. 1995. Passive Microwave Remote Sensing of Land--Atmosphere Interactions. VSP.

Choudhury BJ, Tucker CJ. 1987. Monitoring global vegetation using Nimbus-7 37 GHz Data Some empirical relations. Int J Remote Sens. 8:1085–1090.

Du J, Kimball JS, Jones LA, Watts JD. 2016. Implementation of satellite based fractional water cover indices in the pan-Arctic region using AMSR-E and MODIS. Remote Sens Environ. 184:469–481.

Kerr YH, Njoku EG. 1993. On the use of passive microwaves at 37 GHz in remote sensing of vegetation. Int J Remote Sens. 14:1931–1943.

Lacava T, Brocca L, Coviello I, Faruolo M, Pergola N, Tramutoli V. 2015. Integration of Optical and Passive Microwave Satellite Data for Flooded Area Detection and Monitoring. In: Lollino G, Arattano M, Rinaldi M, Giustolisi O, Marechal J-C, Grant GE, editors. Eng Geol Soc Territ - Vol 3 [Internet]. Cham: Springer International Publishing; p. 631–635.

Li X, Takeuchi W. 2016. Land Surface Water Coverage Estimation with PALSAR and AMSR-E for Large Scale Flooding Detection. Terr Atmospheric Ocean Sci. 27:473.

LI Xi, Wataru TAKEUCHI. 2014. Flood analysis and forecasting by spatio-temporal data mining based on historical satellite image database.

LI Xi, Wataru Takeuchi. Flood event detection by AMSR-E and PALSAR on global scale [Internet]. In: Institute of Industrial Science, The University of Tokyo, Japan. Available from: http://wtlab.iis.u-tokyo.ac.jp/en/images/research_poster/li_poster.pdf

Paloscia S, Macelloni G, Santi E, Koike T. 2001. A multifrequency algorithm for the retrieval of soil moisture on a large scale using microwave data from SMMR and SSM/I satellites. IEEE Trans Geosci Remote Sens. 39:1655–1661.

Singh Y, Ferrazzoli P, Rahmoune R. 2013. Flood monitoring using microwave passive remote sensing (AMSR-E) in part of the Brahmaputra basin, India. Int J Remote Sens. 34:4967–4985.

Sippel SJ, Hamilton SK, Melack JM, Choudhury BJ. 1994. Determination of inundation area in the Amazon River floodplain using the SMMR 37 GHz polarization difference. Remote Sens Environ. 48:70–76.

Takeuchi W, Gonzalez L. 2009. Blending MODIS and AMSR-E to predict daily land surface water coverage. In: Proc Int Remote Sens Symp ISRS Busan Korea. Vol. 29.

Tanaka M, Sugimura T, Tanaka S, Tamai N. 2003. Flood–drought cycle of Tonle Sap and Mekong Delta area observed by DMSP-SSM/I. Int J Remote Sens. 24:1487–1504.

Temimi M, Leconte R, Brissette F, Chaouch N. 2007. Flood and soil wetness monitoring over the Mackenzie River Basin using AMSR-E 37GHz brightness temperature. J Hydrol. 333:317–328.

Watts JD, Kimball JS, Jones LA, Schroeder R, McDonald KC. 2012. Satellite Microwave remote sensing of contrasting surface water inundation changes within the Arctic–Boreal Region. Remote Sens Environ. 127:223–236.

Xi L, Takeuchi W. 2015. Development of large scale flooding detection method by integrating historical global record using AMSR-E/AMSR2 with PALSAR. In: 2015 IEEE Int Geosci Remote Sens Symp IGARSS; p. 822–825.

Zheng W, Liu C, Xin Z, Wang Z. 2008. Flood and waterlogging monitoring over Huaihe River Basin by AMSR-E data analysis. Chin Geogr Sci. 18:262–267.